A 45-dB, 150-Hz, and 18-mW Touch Controller for On-Cell Capacitive TSP Systems

Yeong-Shin Jang, Young-Hun Ko, Jung-Min Choi, Hyung-Seog Oh, and Sang-Gug Lee, *Member, IEEE*

***Abstract*—A touch controller is proposed for on-cell capacitive touch screen panel systems, which adopts a newly proposed peaking noise detector and low-frequency rejection filters. Implemented in a 0.35-μm CMOS, the proposed touch controller with 3.3-V drive signal shows the maximum signal-to-noise ratio and scan rate of 45 dB and 150 Hz, respectively, while consuming 18 mW from a 3.3-V supply.**

***Index Terms*—Embedded-type touch screen panel (TSP), noise detector, on-cell TSP, touch controller.**

I. Introduction

THE demand for touch screen panel (TSP) technology is ever increasing in the information display systems of today, such as mobile phones, tablet PCs, navigation devices, portable media players, digital cameras, and notebook PCs, due to its intuitive user interfaces. Among various TSP technologies, capacitive TSPs become the most popular type because of excellent optical transparency, multi-/soft-touch functionality and reliability. The add-on-type TSPs, which are manufactured by the lamination process in combining the display and TSP panels, have been used widely. Recently, interest in the on- and in-cell TSP technologies has been rapidly increasing as a lower cost and smaller form factor solution [1], [2]. The on- and in-cell technologies (embedded type) include the TSP inside the display panel itself, by embedding the TSP on the color filter and/or in the common plate of liquid-crystal display, which removes lamination process, reduces test cost, and simplifies the supply chain.

With all capacitive TSPs, since the capacitive touch objects such as fingers are capacitive, the three-wave-lamp and battery charger noises can be injected into the touch system through the touch entity. Therefore, the capacitive TSPs require a high-performance touch controller with a high signal-to-noise ratio (SNR) and reporting rate while consuming a small amount of power. With embedded-type TSPs, due to the closer distance between the touch function layer and the display panel, the parasitic capacitances increase, and the noise injection from the display panel becomes stronger into the touch function layer. However, the distance between touch entity and touch function layers becomes wider, which leads to the smaller amount of change in capacitance by a touch entity. Consequently, the smaller decremental change in capacitance and the higher noise lead to more SNR degradation in the embedded-type TSPs. Therefore, a touch controller with higher SNR and noise signal robust is required for the embedded-type TSPs.

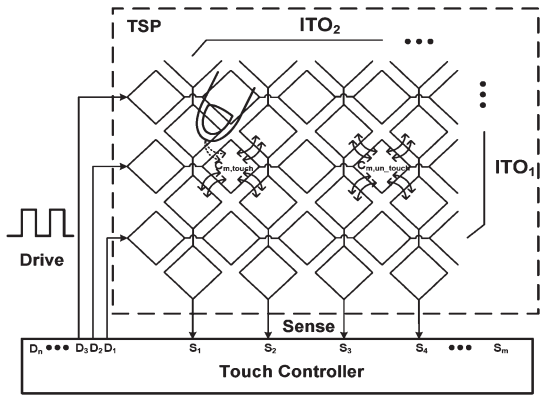

Fig. 1. Conventional capacitive TSP system.

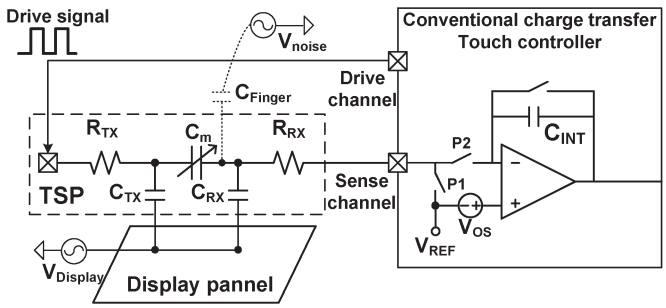

Fig. 2. Equivalent circuit of TSP and noise source model in combination with the conventional charge-transfer-type touch controller.

Fig. 1 shows conventional capacitive TSP system configuration. In Fig. 1, the TSP generally consists of drive $(\mathrm{D_1}-\mathrm{D_n})$ and sense $(\mathrm{S_1}-\mathrm{S_m})$ channels and is sequentially driven by the touch controller. The drive signal goes through the TSP and is then sensed by the same touch controller. The mutual capacitance (C_m), which is formed between $\mathrm{ITO_1}$ and $\mathrm{ITO_2}$ of the TSP, is changed by the touch entity (finger), and the magnitude of the sense signal also changes. This process allows detecting the decremental change in C_m at the touch point; thus, multitouch detection can be accomplished.

Fig. 2 shows the equivalent circuit of TSP and noise source model in combination with the conventional charge-transfer-type touch controller. The charge-transfer-type integrator is widely used in the touch controller to sense the change in capacitance [3]. In Fig. 2, the integrator output can be given by

$$V_{\mathrm{out}} = \frac{C_m}{C_{\mathrm{INT}}} \cdot V_{\mathrm{drive}} + \frac{C_{\mathrm{RX}}}{C_{\mathrm{INT}}} \cdot V_{\mathrm{OS}} \tag{1}$$

Manuscript received February 18, 2014; revised May 10, 2014; accepted July 30, 2014. Date of publication August 5, 2014; date of current version October 1, 2014. This work was supported by the Ministry of Education, Science Technology and the Korea Institute for Advancement of Technology through the Human Resource Training Project for Regional Innovation. This brief was recommended by Associate Editor K.-H. Chen.

The authors are with the Nano Integrated Circuit Expertise Laboratory, Department of Information and Communications Engineering, Korea Advanced Institute of Technology, Daejeon 305-701, Korea (e-mail: kbsh7@kaist.ac.kr).

Color versions of one or more of the figures in this brief are available online at http://ieeexplore.ieee.org.

Digital Object Identifier 10.1109/TCSII.2014.2345292

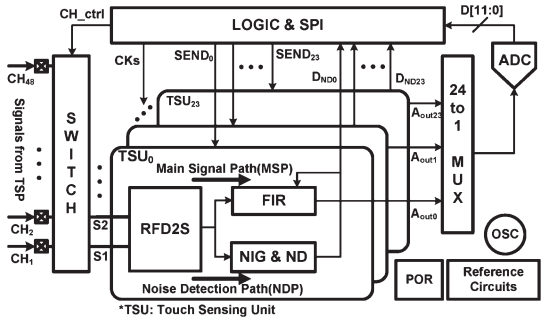

Fig. 3. Proposed touch controller architecture.

where $C_{\rm INT}$, $V_{\rm drive}$, and $V_{\rm OS}$ represent the feedback capacitance of the integrator, the amplitude of the drive signal, and the offset voltage of the amplifier, respectively. $V_{\rm drive}$ is the amplitude of the drive signal, which is normally the same as supply voltage but could be of higher amplitude when charge pump or external high voltage is used to increase SNR. However, the dynamic range is strictly limited not by the drive voltage but by the supply voltage of the circuit. As an example, if $C_{\rm RX}$ in Fig. 2 is around 100–300 pF, an offset of 20 mV in the integrator leads to 0.2–0.5 V dc at the output when $C_{\rm INT}$ is 10 pF. Therefore, the charge transfer type is not suitable for the TSPs with large $C_{\rm RX}$ such as the on-cell TSP as the dynamic range of the integrator is limited easily. Since the integrator accumulates the input signals to achieve a finite-impulse response (FIR) characteristic, the dynamic range reduction becomes more significant in practice. To increase the dynamic range, larger $C_{\rm INT}$ is desirable at the cost of gain reduction and chip size.

The change in C_m (ΔC_m) by a touch is normally around 10% in an on-cell TSP. Since the charge-transfer-type integrator integrates the whole charge of the C_m, the maximum output voltage change by a touch is limited, as given by

$$\Delta V_{\rm out,max} = \frac{1}{2} \cdot V_{DD} \cdot \frac{\Delta C_m}{C_m} \tag{2}$$

where V_{DD} represents supply voltage, such that $\Delta V_{\rm out,max}$ is only around 160 mV if the V_{DD} is 3.3 V. Small change in the output voltage limits SNR. In Fig. 2, the input signal of the touch controller that goes through TSP can easily be degraded by the common-mode noises such as the display noise, which leads to the SNR degradation.

This brief proposes a high-SNR touch controller architecture that adopts resistive-feedback differential-to-single-ended amplifier (RFD2S) for input stage of the touch sensing circuit to overcome the conventional charge-transfer-type integrator issues and a noise detector to avoid peaking noises such as three-wave-lamp and battery charger noises.

II. Proposed Touch Controller Design

Fig. 3 shows the proposed touch controller architecture. In Fig. 3, the differential sensing scheme (2-to-1 MUX) allows lower power consumption for the proposed touch controller since the controller uses only 24 touch sensing units (TSU) for the 48 sense channels. As a result, the required number of TSUs is only half of that of a conventional sensing system that adopts charge transfer integrators. Each amplifier, the class AB type [4], in TSU consumes only 60 μW; and its unit-gain bandwidth and phase margin are 3 MHz and 60°, respectively.

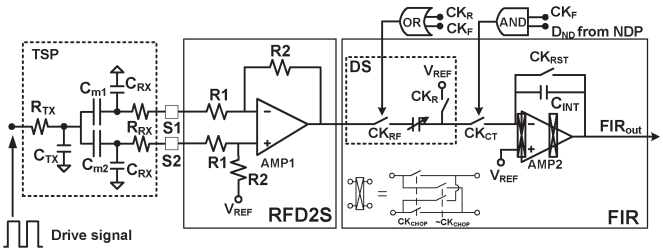

Fig. 4. Circuit details of the main signal path in Fig. 3.

The overall static power consumed by all the amplifiers in TSU is 60 μW $\times$ 3 $\times$ 24 = 4.32 mW.

The differential sensing removes the common display noise. In Fig. 3, there are two signal paths in the TSU, namely, the main signal path and the noise detection path, which consist of RFD2S + FIR and RFD2S + NIG + ND blocks, respectively. The proposed touch controller solves the noise issues by dividing the noises into low-frequency and peaking (high-frequency) types. The low-frequency noises are suppressed by the filters in the main signal path. Under the presence of peaking noises, the noise detection path detects and transfers the information to the main signal path, such that the main signal path would skip the corresponding input signal.

In Fig. 4, the frequency chopping technique is adopted in the AMP2 in order to remove the amplifier offset, and the chopping frequency ($\rm CK_{CHOP}$) is the half of the frequency of the drive signal. The chopping frequency (~150 kHz) is wider than the input signal bandwidth (~100 Hz), which is carried by the drive signal (~300 kHz). The frequency response is similar in both with and without chopping technique since signal aliasing is negligible.

The RFD2S block (with default value of R1 and R2 being 1 and 20 kΩ, respectively) in Fig. 4, as an input stage, achieves high gain without the dynamic range degradation by three reasons in comparison with conventional charge-transfer-type integrator. First, the amplifier offset is not amplified, and second, the RFD2S block amplifies only the difference in C_m of the adjacent channels, not the absolute value of C_m, so that the dynamic range reduction issue can be avoided. As a result, the maximum output voltage change by the touch at the FIR block becomes $\pm V_{DD}/2$. Furthermore, the RFD2S block can removes common-mode noise such as display noise due to differential characteristic. Although a fully differential charge-transfer-type integrator can reject the common-mode noise by the differential output, the voltage swing of the two outputs can be reduced in case of a large common-mode noise signal, leading to dynamic range degradation. However, in the proposed RFD2S block shown in Fig. 4, the common-mode noise that is applied at the noninverting and inverting input is cancelled at the output. Therefore, there is no dynamic range reduction issue.

In Fig. 4, the RFD2S block differentiates the input signal and, thereby, suppresses the low-frequency noises such as three-wave-lamp noise (~47 kHz). Then, the FIR block converts the input signal down to dc and provides low-pass filtering characteristic. Then, the FIR block converts the input signal down to dc and provides low-pass filtering characteristic. The clock timing diagram of the proposed touch controller is shown in Fig. 5 ($\rm CK_{COMP}$ is explained later). In the main signal path, the RFD2S output at the rising and falling timing of drive signal is sampled by $\rm CK_{RF}$ (the OR combination of $\rm CK_R$ and

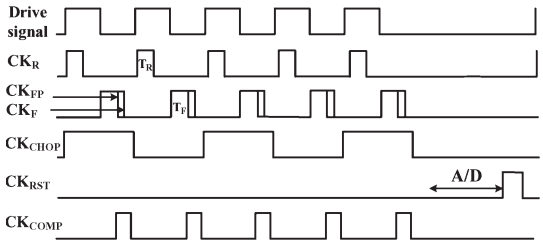

Fig. 5. Clock timing diagram of the proposed touch controller.

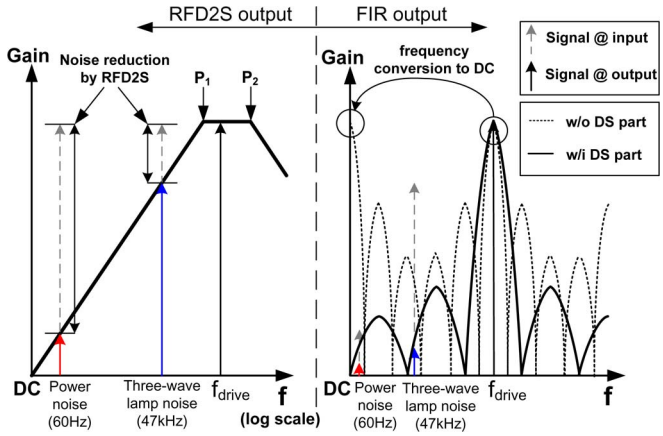

Fig. 6. Frequency response at the output of the RFD2S and FIR blocks.

$\mathrm{CK_F}$). The two sampled signals are subtracted and transferred by $\mathrm{CK_F}$ (if $D_{\mathrm{ND}} =$ '1'). After analog-to-digital conversion, the FIR block is reset by $\mathrm{CK_{RST}}$. If the three-wave-lamp noise has a large amount of frequency harmonics, the SNR could be degraded, which has not been considered in this work. The differentiating sample (DS) part of the FIR block samples the outputs of the RFD2S block two times, at the rising $(\mathrm{T_R})$ and falling $(\mathrm{T_F})$ edges of the input signal, and the charge difference of the two sampled signals is transferred to the following stage, through which the dc-offset and low-frequency noises of prior stages are suppressed.

The transfer functions of the RFD2S in Fig. 4 are given by

$$H_1(s) = \frac{s \cdot R_2 \cdot \Delta C_m}{(1 + s \cdot R_1 \cdot C_m) \cdot (1 + S \cdot R_{\mathrm{RX}} \cdot C_{\mathrm{RX}})} \quad (3)$$

where ΔC_m C_{RX}, and R_{RX} represent the change in C_m by the touch, total capacitance, and total resistance of the sensing line, respectively. Since R_{RX}, C_{RX}, R_1, and C_m make first- and second-frequency poles ($\mathrm{P_1}$ and $\mathrm{P_2}$ in Fig. 6), the overall transfer function of the RFD2S with TSP actually shows bandpass characteristic, as shown in Fig. 6. Therefore, both low- and high-frequency noises can be suppressed. The resistor string with switches is used for an adjustable R1 and R2. In practice, the resistor value is manually set depending on TSP load condition. The filter band could be changed by the TSP location. It can cause location-to-location SNR variation, which is usually less than 3 dB.

The output of the RFD2S block is sampled by the FIR block, which accumulates the drive signals and rejects noise signals, with transfer function given by

$$H_2(s) = \frac{C_m}{C_{\mathrm{INT}}} \sum_{i=1}^{N_{\mathrm{PDA}}} \left\{ \left(e^{j2\pi f/f_{\mathrm{drive}}}\right)^{-i} - \left(e^{j2\pi f/f_{\mathrm{drive}}}\right)^{-i/2} \right\} \quad (4)$$

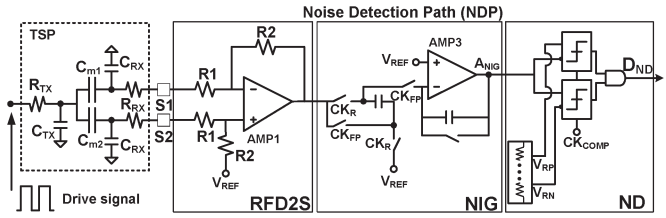

Fig. 7. Circuit details of the noise detection path in Fig. 3.

where C_{INT}, N_{PDA}, and f_{drive} represent the feedback capacitance of the FIR block, the number of the predetermined accumulation in the FIR block, and the drive signal frequency, respectively. As can be seen from (4), the difference of the sampled signals at the rising and falling timing of the drive signal (done by the DS part) implies high-pass filtering operation, which suppresses the low-frequency noises. The N_{PDA} times accumulation of this action (done by the FIR block) achieves low-pass filtering characteristic with $k \cdot f_{\mathrm{drive}}/N_{\mathrm{PDA}}$ of null frequencies $(k = 1, 2, \ldots, N_{\mathrm{PDA}})$, converting 300, 900, 1500 kHz, etc., down to dc.

Fig. 6 shows the frequency response of the FIR block as well. The drive signal that passes through RFD2S is filtered by the FIR block, and the noises are filtered two times by the bandpass and low-pass filtering characteristics with nulls at the multiples of $f_{\mathrm{drive}}/N_{\mathrm{PDA}}$. In Figs. 4 and 5, since the frequency of the drive signal is the same as that of the switch signal in the FIR block, the drive signal is downconverted to dc, whereas the noise (for example, ~50 kHz) is converted to the null frequency shown in Fig. 6 by adjusting N_{PDA}, respectively. Consequently, the main signal path accumulates wanted signal but suppresses noises, which leads to the higher SNR. Since the drive signal is downconverted to dc, the postprocessing after analog-to-digital conversion becomes simple. As shown in Fig. 6, the drive signal (300 kHz) is downconverted to dc regardless of the presence of the DS part. However, the low-frequency noises, the power, and the three-wave-lamp noises could be suppressed more due to the DS part than the case of normal 300-kHz sampling. In addition, since the DS part samples the drive signal effectively at 600 kHz, which is twice the normal 300-kHz sampling, the signal strength at the input of the FIR block doubles, leading to improved SNR. However, the low-pass filtering characteristic of the FIR block could be inferior to that of the normal 300-kHz sampling, as indicated by the wider null-to-null frequency shown in Fig. 6.

The circuit details of the noise detection path (NDP) in Fig. 3 is shown in Fig. 7. As shown in Fig. 3, the RFD2S block is shared with the main signal path. From Fig. 7, the summation of the outputs of RFD2S, which are sampled at $\mathrm{T_R}$ and $\mathrm{T_F}$ falling edges of the input signal, is expected to be symmetric at the output of noise indicator generation (NIG) block $(\mathrm{A_{NIG}})$. However, under the presence of the peaking noises, the symmetry of the two sampled signals will be disrupted. In the noise detection path, since the NIG block adds the two outputs of the RFD2S, $\mathrm{A_{NIG}}$ becomes nonzero under the presence of peaking noises, which can be used as a noise indicator.

The method of detecting peaking signal amplitude that suppresses the peaking noise has been also reported in [5]. However, in [5], it is difficult to determine the noise threshold level because the signal amplitude for the noise detection depends on the TSP types and sensor gain. In addition, the threshold level

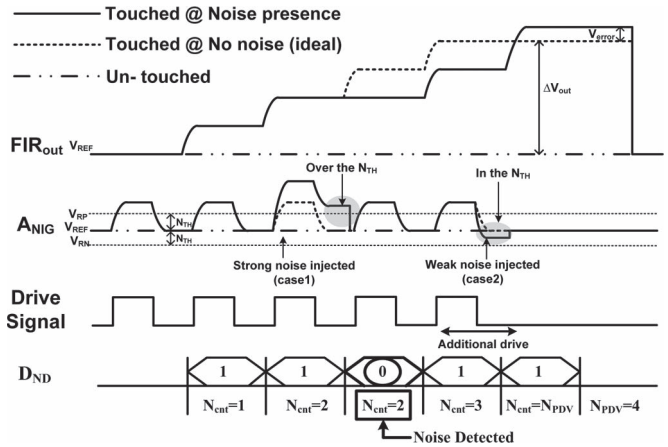

Fig. 8. Example of the analog outputs of TSU.

should be higher than the maximum input signal amplitude plus the noise margin, meaning that the noise signals with amplitude smaller than three times the amplitude of the touched signal could not be detected. Therefore, the technique reported in [5] does not respond to noise signals with amplitude comparable touch signal, limiting the SNR improvement. Using noise indicator, the proposed noise detection technique provides more accurate sensing for the presence of peaking noise independent of the TSP types and sensor gain because it utilizes the differential characteristic of the signals sampled at the T_R and T_F edges of input signal. In other words, the noise indicator level is always V_{REF} if there is no noise. However, the proposed noise detection method can skip small values of noises by controlling the noise threshold level.

A_{NIG} is evaluated by the comparators in the noise detector (ND) block at the rising edge of the CK_{COMP} whether it is located between positive (V_{RP}) and negative (V_{RN}) reference voltages or not. If $V_{RN} < A_{NIG} < V_{RP}$, the output of the ND block (D_{ND}) becomes 1. If not, $D_{ND} =$ '0', in which case, the CK_{CT} in the FIR block turns OFF, such that the corresponding input signal would not be accumulated at the output of the FIR block. Therefore, the FIR block can avoid the signal contaminated by the peaking noise. By the LOGIC block shown in Fig. 3, the accumulation of the input signal continues until the total number of accumulated signal becomes equal to N_{PDA} by counting $D_{ND} =$ '1'.

Fig. 8 shows an example of the analog outputs of TSU depending on the presence or not of noise for $N_{PDA} = 4$. In case of untouched condition, there is no change at output of FIR block (FIR_{out}). When TSP is touched and if there is no noise, the analog output gradually increases by N_{PDA} times (dashed line). However, if a strong noise is injected (case1 in Fig. 8), the A_{NIG} surpasses the reference voltage (V_{REF}) by more than the noise threshold level (N_{TH}), in which case D_{ND} becomes 0. Therefore, the FIR block skips the corresponding input signal, so that the FIR block output also keeps the previous value, and the number of accumulated signal (N_{CNT}) does not increase. Although the noise is injected, if its level is not higher than N_{TH} (case2 in Fig. 8), the FIR block accumulates the corresponding input through the main signal path. If the noise threshold level (N_{TH}) is too small, the SNR will increase, but the sensing time can be increased by the detection of even small noise signals. Therefore, SNR and reporting rate can be traded off by controlling N_{TH}.

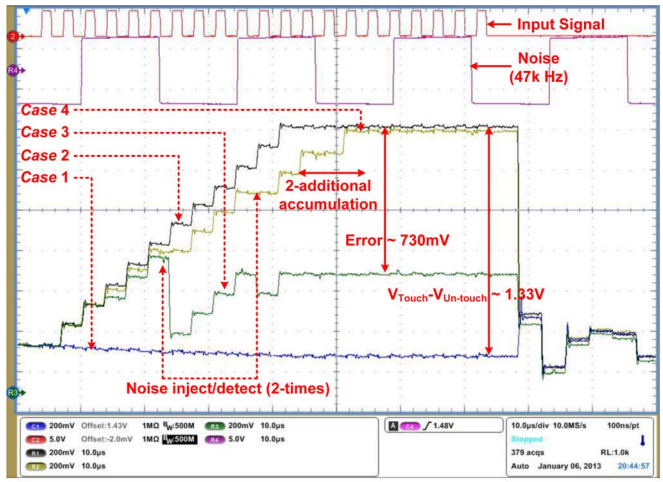

(a)

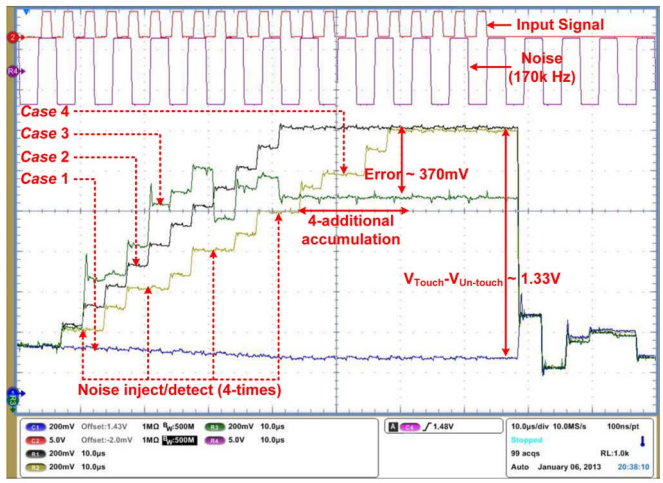

(b)

Fig. 9. Measured output of the FIR block for cases 1–4 under (a) 47-kHz and (b) 170-kHz noises.

III. Measurement Results

The proposed touch controller shown in Fig. 3 is designed to dissipate 18 mW from a 3.3-V supply, based on a 0.35-μm CMOS technology, and evaluated using 10.1-in on-cell TSP. Fig. 9 shows the measured output of the FIR block for the cases of untouched (*case* 1), touched under no noise (*case* 2), touched under the presence of 47- and 170-kHz noise with ND block turned OFF (*case* 3) or ON (*case* 4) conditions. In Fig. 9, the noise sources, 47 and 170 kHz, are similar in terms of frequencies to the three-wave-lamp and one of the charger noises, which are applied to the touch object (finger) directly. As shown in Fig. 9, with *case* 3, the injection of the peaking noise induces distortion in the measured output of the FIR block. However, by turning ND block ON, in *case* 4, the measured output of the FIR block accumulates to the value similar to that of *case* 2, by skipping the distorted signals and additionally accumulating the input of signals. In Fig. 9, under the presence of the noise, in *case* 3, the output codes along the same sense line fluctuate, whereas the output codes become stable in *case* 4, such as in *case* 2, demonstrating the proper sensing of the touch position by the proposed touch controller scheme. In Fig. 9, the output differences between cases 1 and 2 and cases 1 and 4 are the same with the value of 1.33 V.

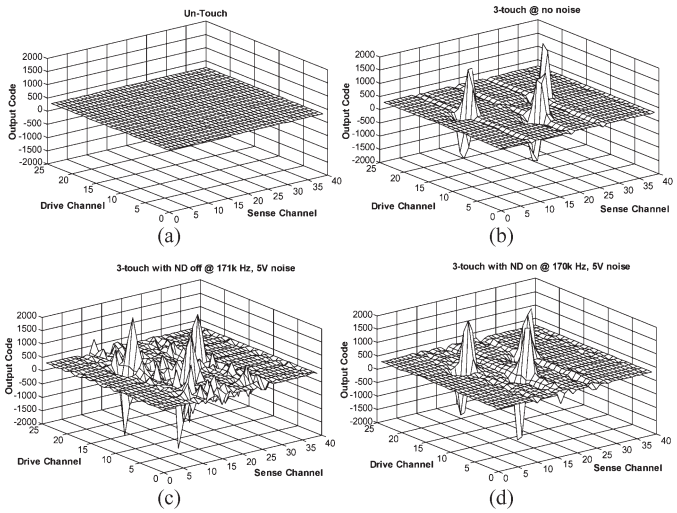

Fig. 10. Three-dimensional images of the measured output code for cases (a) 1, (b) 2, (c) 3, and (d) 4 under the presence of 170-kHz/5-V noise.

TABLE I
PERFORMANCE SUMMARY

Sensor Type	On-cell Capacitive	
ITO Pattern	Diamond Pattern	
Channel	1000 channels (Driving: 40, sensing:25)	
Pattern Pitch	4.5 mm	
Sensing Method	Mutual	
Processor	Cortex M3	
Driving Voltage	3.3 V	
Maximum Reporting Rate	ND Off	150 Hz
Maximum SNR	Normal display	45 dB
	ND off (@ 5V-170kHz noise)	12 dB
	ND on (@ 5V-170kHz noise)	32 dB
Power Consumption	9.6 mW	Analog: 7 mW
		Digital: 11 mW

Fig. 10 shows the 3-D images of the measured output code for cases 1, 2, 3, and 4 under the presence of 170-kHz/5-V noise. As can be expected from the results in Fig. 9, Fig. 10(a) and (b) shows clear touch function and SNR of 45 dB. In Fig. 10(c), the noise degrades the SNR to 12 dB, whereas SNR of more than 32 dB is achieved by turning the ND block ON, as shown in Fig. 10(d). Since the input is differential, the output codes show differential $(\pm)$ characteristics with a value of around $(\pm)1900$ LSB of 12 b 500-kS/s SAR ADC, which consumes 500 μW.

Table I summarizes the specifications and performances of the proposed touch controller. As can be seen in Table I, the proposed touch controller shows maximum reporting rate of 150 Hz and SNR of 45 dB when the display is turned on. The static performance of a touch controller can be characterized through SNR, which is given by [6]

$$\mathrm{SNR(dB)} = 20\log\left(\frac{\mathrm{TStrength}}{\mathrm{NT_{RMS100}}}\right) \tag{5}$$

where

$$\mathrm{TStrength} = \mathrm{ST_{AVG100}} - \mathrm{SUT_{AVG100}} \tag{6}$$

$$\mathrm{NT_{RMS100}} = \sqrt{\frac{\sum_{n=0}^{n=99}\left(\mathrm{Data}[n] - \mathrm{ST_{AVG100}}\right)^2}{100}}. \tag{7}$$

TStrength, ST, SUT, and NT represent touch strength, signal touched, signal untouched, and noise touched, respectively. AVG100 and RMS100 denote the simple numeric average of 100 data points and the root mean square of 100 data points of AVG100, respectively. AVG100 and RMS100 are evenly sampled over a period of 500 frames. Table II shows the key performance summary of the proposed touch controller in comparison with prior works. The proposed touch controller shows the best SNR and scan rate, which can be a solution for the on-cell capacitive TSPs. Fig. 11 shows the microphotograph of the proposed touch controller with a chip size of 3350×3400 μm^2.

TABLE II
PERFORMANCE COMPARISONS

	[1]*	[2]	[3]	[5]	This Work
Power (mW)	19.5	19	19	18.7	**18**
Cap-TSP type	on-cell	on-cell	add-on	add-on	**on-cell**
# of Channels	(9+15)*	53x29	16x20	43x27	**40x25**
Maximum SNR (dB)	36	12.6	24	39	**45**
Reporting rate (Hz)	120	140	65	120**	**150****
Silicon area (mm^2)	4.5x0.8	4x5	4	10.4	**3.4x3.4**
Technology (nm)	90	350	180	350	**350**

* single/dual touch available, ** scan-rate

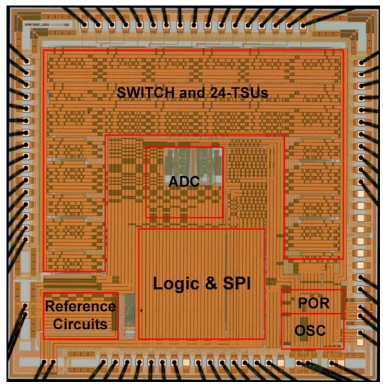

Fig. 11. Chip microphotograph.

IV. CONCLUSION

A touch controller has been proposed for on-cell capacitive TSP systems. The proposed touch controller can achieve a high SNR by adopting an RFD2S amplifier as an input stage to overcome the issues of the conventional charge-transfer-type integrator and a noise detector to avoid peaking noise such as three-wave-lamp and battery charger noises. Implemented in a 0.35-μm CMOS, the proposed touch controller exhibited a maximum scan rate and an SNR of 150 Hz and 45 dB, respectively, when both the supply voltage and amplitude of the drive signal are 3.3 V, which are evaluated using a 10.1-in on-cell capacitive TSP. The proposed touch controller consumes 18 mW from a 3.3-V supply and can recognize multitouch events.

REFERENCES

[1] H.-R. Kim *et al.*, "A mobile-display-driver IC embedding a capacitive touch-screen controller system," in *Proc. IEEE ISSCC*, Feb. 2010, pp. 114–116.
[2] I.-S. Yang and O.-K. Kwon, "A touch controller using differential sensing method for on-cell capacitive touch screen panel systems," *IEEE Trans. Consum. Electron.*, vol. 57, no. 3, pp. 1027–1032, Aug. 2011.
[3] S. Ko *et al.*, "Low noise capacitive sensor for multi-touch mobile handset's applications," in *Proc. IEEE Asian Solid-State Circuits Conf.*, Nov. 8–10, 2010, pp. 1–4.
[4] R. Hogervorst, J. P. Tero, R. G. H. Eschauzier, and J. H. Huijsing, "A compact power-efficient 3 V CMOS rail-to-rail input/output oerational amplifier for VLSI cell libraries," *IEEE J. Solid-state Circuits*, vol. 29, no. 12, pp. 1505–1513, Dec. 1994.
[5] J.-H. Yang *et al.*, "A highly noise-immune touch controller using filtered-Delta-integration and a charge-interpolation technique for 10.1-in capacitive touch-screen panels," in *Proc. IEEE ISSCC*, Feb. 2013, pp. 390–391.
[6] *Touch Sensors Design Guide, 10620D-AT42*, ATMEL Corporation, San Jose, CA, USA, Sep. 2004.